Theory of scanning-tunneling-microscopy images of intercalated graphite surfaces

Xiao-rong Qin and George Kirczenow

Department of Physics, Simon Fraser University, Burnaby, British Columbia, Canada V5A 1S6

(Received 20 November 1989)

The electronic and structural properties of intercalated graphite surfaces imaged with scanning tunneling microscopy (STM) have been studied theoretically, with use of a modification of the tight-binding model of Blinowski *et al.* The corrugation amplitude (CA) and carbon-atom site asymmetry (CSA) are sensitive to the number, m, of graphite layers covering the first guest layer, to the amount of transferred charge and its distribution to the surface subband structure. The CA and CSA can be used to map the stage domains across a freshly cleaved surface. The CSA has a surprising dependence on the charge transfer and on m. We explain the unusual absence of atomic scale features in the STM images of BiCs-graphite reported by Gauthier *et al.* The STM images of the surfaces of both donor and acceptor graphite intercalation compounds are discussed.

I. INTRODUCTION

The scanning-tunneling-microscopy (STM) image of a pristine graphite surface at low bias voltage has two remarkable features,[1,2] a large corrugation in the tunneling current over the center of each carbon hexagon, and a pronounced asymmetry in the current between adjacent carbon-atom sites.[1-8] As was shown by Tersoff,[5] the fundamental reason for the corrugation is that the STM probes the local electron density of states at the Fermi level. Since the Fermi surface of graphite is very small, the STM image is a reflection of the spatial dependence of the wave functions of just a few electron states, and the current "hole" at the center of each hexagon is due to a node in the wave functions of the Fermi electrons.[5] Batra *et al.*[6] and Tománek and co-workers[7,8] have shown that the carbon-atom site asymmetry is a property of the electron eigenstates resulting from the AB stacking of the hexagonal layers of carbon atoms.[6-8] The electronic properties of graphite can be modified systematically by intercalating various guest species into the galleries between the carbon layers. While the physics of graphite intercalation compounds (GIC's) has attracted a great deal of attention in recent years,[9,10] their surface properties remain largely unexplored. The STM should be an excellent probe for these surfaces, and indeed some interesting experimental[11-14] and theoretical[8,15] work has recently begun to appear. But the lack of a comprehensive theory makes it difficult to interpret much of the data. In this paper we present the first theory of the STM images of GIC surfaces, which is applicable to both donor and acceptor intercalate species and to staged structures.[16] We show that the corrugation amplitude and the carbon-atom site asymmetry are sensitive to the charge transfer between the guest and host, to the distribution of the transferred charge among the host layers close to the surface, and to the near-surface band structure. Based on this, it should be possible to use the STM to map out the pattern of stage domains at a GIC surface. Even in the bulk case, there are important unanswered questions about the domain structure and

electronic properties of GIC's,[9,10] which make such surface studies all the more interesting. A surprising prediction of our theory is that in many cases there should be *no* carbon-atom site asymmetry in the STM image even when the usual AB stacking of the graphite layers occurs at the GIC surface, and that the asymmetry should switch on *discontinuously* with decreasing charge transfer. We also predict that donor GIC's should have stronger carbon-atom site asymmetries than acceptor GIC's with the same absolute value of the charge transfer per carbon atom. We present a possible explanation of the remarkable absence of atomic-scale features in the STM images of BiCs-graphite reported by Gauthier *et al.*[11]

We briefly summarize the structure of graphite intercalation compounds in Sec. II. Our theoretical model is described and analyzed in Sec. III. The results are presented in Sec. IV. Finally, we outline our conclusions in Sec. V.

II. GIC STRUCTURE

When a layered host material such as graphite is intercalated with a guest species, the guest atoms fill some of the galleries between the host layers, leaving others empty. The new ordered structure has a period consisting of a guest layer followed by n graphite host layers. This is called a stage-n compound.

The characteristic structure of a GIC is represented in Fig. 1 which shows a slice through the crystal perpendicular to the host layers. Figure 1 shows a stage-4 compound with every fourth gallery occupied by the guest, but the crystal is divided into Daumas-Hérold domains with different galleries being occupied by the guest in adjacent domains.[17] In this paper we will discuss surfaces such as the top surface in Fig. 1, where the number m of graphite layers covering the guest layer closest to the surface depends on the particular domain involved. These m surface graphite layers are very different from ordinary pristine graphite. It is known that the formation of GIC's is accompanied by charge-transfer and screening
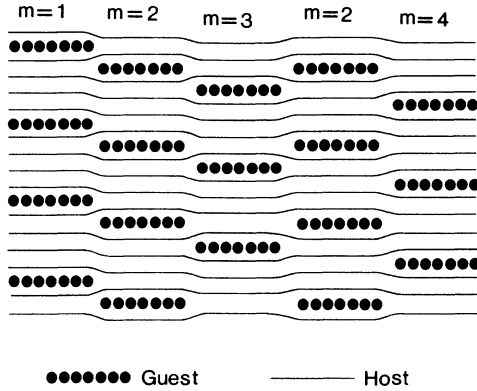
FIG. 1. Schematic representation of stage order and domain structure in a stage-4 GIC.

effects. The electrons (holes) which are transferred to the graphite from the donor (acceptor) guest screen the charged guest layers, and their concentration is highest in the graphite layers closest to the guest. Because of the unusual band structure of the graphite, the screening is nonexponential, with the screening charge density and the associated potential decaying roughly as a power of the distance from the closest guest layer.[18] Consequently, in the surface region, there are electrostatic potential differences between the m graphite layers, which should be included in the Hamiltonian of the system. In addition, the Fermi level of the system is shifted from that of pristine graphite because of the transferred charge. Clearly, the different (m) surface domains have different potential distributions, energy bands, and Fermi surfaces, and, therefore, STM images which can differ markedly from each other and from that of pristine graphite.

In our model we assume that the stacking sequence of graphite layers, *where it is not interrupted by the presence of a guest layer,* is still the usual graphite $AB\,AB$ stacking sequence. This is known to be correct in the bulk case for most staged GIC's.[9,10] In this stacking there are two kinds of carbon-atom sites: α sites which are adjacent to carbon atom sites in the neighboring graphite layer(s),
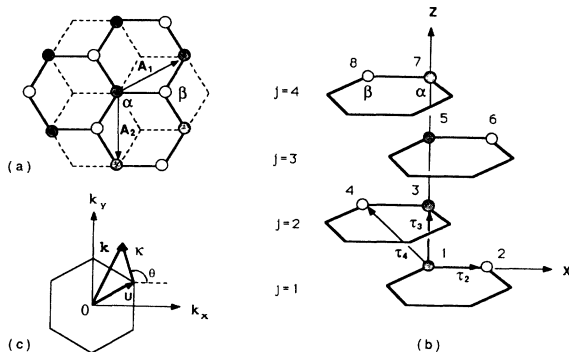

FIG. 2. Graphite AB stacking structure with α- and β-type carbon-atom sites in (a) 2D and (b) 3D perspectives, and (c) the hexagonal 2D Brillouin zone, where wave vector $\mathbf{k}=\mathbf{u}+\boldsymbol{\kappa}$ and $\mathbf{u}=(2\pi/3b,\,2\pi/3^{3/2}b)$.

and β sites which are adjacent to the (vacant) centers of the carbon hexagons in the neighboring layers, as shown in Figs. 2(a) and 2(b).

Experimentally, surfaces such as those shown in Fig. 1 can be prepared by cleaving a GIC sample, and at least in the case of $SbCl_5$-graphite, the surface domain structure appears to be sufficiently stable to be studied in vacuum, according to the high-resolution scanning-ion-microprobe work of Levi-Setti *et al.*[19] Laguës, Marchand, and Frétigny[20] have suggested that some guest species may tend to segregate towards the surface, leading to an increased guest concentration in the first subsurface gallery, while the opposite effect may occur for other guests. Our theory is applicable also to such systems, as well as to graphite monolayers and multilayers on clean metal surfaces.

III. THE THEORETICAL MODEL

Our starting point is the result of Tersoff and Hamann,[21] that at low bias voltages, for a simple s-wave model of the STM tip, the tunneling current is proportional to the local density of states at the Fermi energy E_F which is given by

$$\rho(\mathbf{r},E_F)=\sum_{\mathbf{k},n}|\Psi_{\mathbf{k}n}(\mathbf{r})|^2\,\delta(E_{\mathbf{k}n}-E_F)\ ,$$

where r is the center of curvature of the tip and $\Psi_{\mathbf{k}n}$ and $E_{\mathbf{k}n}$ are the electron eigenstates and energy eigenvalues of the sample. The STM image in the constant-current mode represents a contour of constant $\rho(\mathbf{r},E_F)$.

To calculate $\rho(\mathbf{r},E_F)$ for the STM image of a surface domain, we structure the model Hamiltonian of the system so as to include the effects of transferred charge distribution, and use a modification of the tight-binding model of Blinowski and co-workers[22] to find the wave functions $\Psi_{\mathbf{k}n}$ of the states near the Fermi energy.

The tight-binding model of Blinowski and co-workers has been used successfully to describe the bulk electronic properties of stated GIC's for the larger guest species. Compared with their model, our tight-binding model uses the same basis states for the wave function $\Psi_{\mathbf{k}n}$ of the system of m graphite layers, but a different form of the Hamiltonian. The m graphite layers in their model are in the bulk of GIC, and they treat the charge-distribution-related Hamiltonian matrix elements phenomenologically. Our interest is in the surface region, and we calculate the charge distribution and hence find its effects on the Hamiltonian matrix elements by numerically solving the nonlinear self-consistent Thomas-Fermi equations of Safran and Hamann.[18]

We note that simple tight-binding models are known to be capable of describing the main features of the STM image of pristine graphite.[8] Our calculations reproduce the results of the published first-principles calculations of the STM images of multilayer slabs of pristine graphite[6] as well as of graphite monolayers[5] with reasonable accuracy. For example, we find an asymmetry of $\sim0.6-0.7$ Å between the α and β sites of a four-layer slab of pristine graphite in constant current mode, which is close to the 0.5 Å found by Batra *et al.*[6] under similar

conditions using a self-consistent pseudopotential method.

A. Potential and charge distribution

The Safran-Hamann Thomas-Fermi theory has, in the past, been found to be adequate for the description of GIC energetics of staging, a phenomenon which is very sensitive to the distribution of the transferred charge.[9,10,18,23] Safran and Hamann derived the nonlinear self-consistent Thomas-Fermi equations and solved them analytically to give the bulk potential distribution in GIC's. We calculate the potential distribution of a surface domain by solving the equations numerically for a semi-infinite GIC with appropriate surface boundary conditions.

Three important approximations are involved in the derivation of the nonlinear self-consistent Thomas-Fermi equations of Safran and Hamann:[18] (a) the transferred charge is homogeneously distributed in the layers perpendicular to the c axis, i.e., both the graphite and the intercalant layers are treated as charged sheets with an inhomogeneous potential along the c axis only; (b) the effects of the small c axis band dispersion of the graphite energy bands are neglected, so that the energy bands can be described by a two-dimensional model; (c) a continuum approximation to represent the distribution between the intercalant layers is adopted.

For donor guests, the Thomas-Fermi energy of the system is then given by[18]

$$E(n_e) = \frac{1}{2}\int eV(z)[n_i(z)-n_e(z)]dz + \int t(n_e)n_e(z)dz \ ,$$

(1)

where $n_i(z)$ and $n_e(z)$ are the intercalate-ion and electron carrier density, respectively, $t(n_e)$ is the total band energy per electron due to the in-plane two-dimensional (2D) graphite band dispersion, $V(z)$ is the potential distribution, and the electron potential energy is $(-e)V(z)$.

The first term in Eq. (1) represents the electrostatic energy, with $V(z)$ satisfying

$$\frac{d^2V(z)}{dz^2} = -\frac{4\pi e}{\epsilon}[n_i(z)-n_e(z)] \ ,$$

(2)

where $\epsilon \cong 5.4$ is the c-axis dielectric constant[18] of graphite layers.

The second term in Eq. (1) is the band kinetic energy of the electron carriers. The graphite band dispersion is given approximately by $\varepsilon(\kappa)=\frac{3}{2}\gamma_0 b|\kappa|$,[22] the energy being measured near the location of the Fermi level of pristine graphite. Here, $b=1.42$ Å is the in-plane nearest-neighbor distance of graphite, κ is the 2D wave vector measured from the corner of the hexagonal 2D Brillouin zone [see Fig. 2(c)], and $\gamma_0=2.51$ eV (Ref. 24) is the tight-binding Hamiltonian matrix element associated with in-plane nearest-neighbor coupling.[22] The total band energy density per electron $t(n_e)$ is then

$$t(n_e) = \frac{2}{3}t_0 n_e^{1/2} \ ,$$

(3)

where $t_0 = \frac{3}{2}\gamma_0 b(\pi c_0)^{1/2}$, and $c_0=3.35$ Å is the interlayer

spacing of graphite.

Based on the Thomas-Fermi approximation, if $t(n_e)$ and $(-e)V(z)$ have their zeros defined by the Fermi level of pristine graphite, the minimization of Eq. (1) with respect to $n_e(z)$ yields[18]

$$eV(z) = t_0 n_e^{1/2}(z) \ ,$$

(4)

and one can rewrite Eqs. (2) and (4) as

$$\frac{d^2\phi(\xi)}{d\xi^2} = \tilde{n}_e(\xi) - \tilde{n}_i(\xi) \ ,$$

(5)

$$\phi^2(\xi) = \tilde{n}_e(\xi) \ ,$$

(6)

where

$$\phi(z) = eV(z) \ ,$$

(7)

$$\tilde{n}_e(\xi) = t_0^2 n_e(z) \ ,$$

(8)

and

$$\xi = (e/t_0)(4\pi/\epsilon)^{1/2} \ .$$

(9)

In the region of graphite layers, we combine Eqs. (5) and (6) to yield

$$\frac{d^2\phi(\xi)}{d\xi^2} = \phi^2(\xi) \ .$$

(10)

Now, let us consider the boundary conditions at the intercalate layers. We define σ, the areal charge density on the intercalate layers, as

$$\sigma = \frac{f}{q/2}\frac{e}{\Omega} \ ,$$

(11)

where f is the number of electrons received or donated per intercalate unit, $q \times n$ is the number of carbon atoms per intercalate unit for a stage-n GIC, which is related to the stoichiometry of GIC's, and $\Omega=3b^2\sin60°$ is the area of the unit cell of 2D graphite. Thus, $2f/q$ is the number of electrons transferred per 2D graphite unit cell on the intercalate layers. Therefore, at the Lth intercalant layer the boundary conditions are given by[18,25]

$$\phi(\xi_L^+) = \phi(\xi_L^-) \ ,$$

(12)

$$\phi'(\xi_L^+) - \phi'(\xi_L^-) = -p \ ,$$

(13)

where $p=2\sigma t_0(\pi/\epsilon)^{1/2}$, and ξ_L^+ and ξ_L^- are locations just above and below the Lth intercalant layer, respectively (see Fig. 3).

Since there is no free areal charge density on the GIC surface, and a GIC should be neutral as a whole, for a semi-infinite GIC we can take the electric field outside the GIC to be zero, so that the surface boundary condition is

$$\phi_s' = 0 \ .$$

(14)

We multiply Eq. (10) by $2\phi'(\xi)$ and integrate over the near surface region $(o \leq \xi \leq s$, see Fig. 3) with the consideration of the surface boundary conditions to obtain

$$\phi'(\xi) = -[\frac{2}{3}(\phi^3(\xi)-\phi_s^3)]^{1/2} \ .$$

(15)

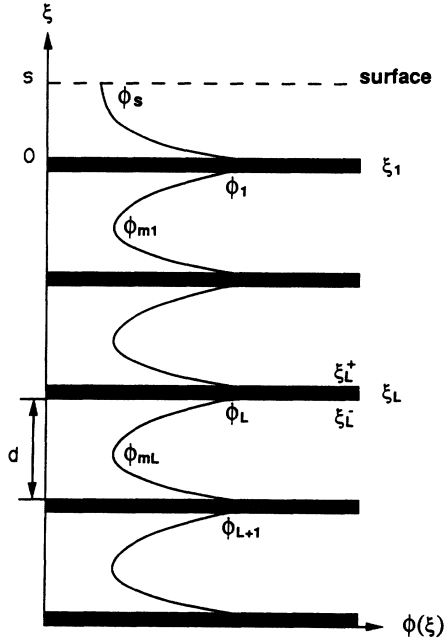Similarly, in the region $\xi_L^- \leq \xi \leq \xi_{L+1}^+$,

FIG. 3. Schematic representation of the charge-transfer-associated potential-energy distribution between intercalant layers and between the surface and the first subsurface intercalant layer.

$$\phi'(\xi) = \pm\{\tfrac{2}{3}[\phi^3(\xi) - \phi_m^3]\}^{1/2}, \tag{16}$$

where ϕ_m is the minimum value of the region.

From (12), (13), and the above Eq. (16), we obtain

$$[\tfrac{2}{3}(\phi_{L+1}^3 - \phi_{mL}^3)]^{1/2} + [\tfrac{2}{3}(\phi_{L+1}^3 - \phi_{mL+1}^3)]^{1/2} = -p. \tag{17}$$

By integrating (15), we find

$$s = (\tfrac{3}{2})^{1/2}\int_{\phi_s}^{\phi_1} d\phi\frac{1}{(\phi^3 - \phi_s^3)^{1/2}}, \tag{18}$$

where s is the distance from the first intercalant layer to the surface. Similarly, from (16)

$$d = (\tfrac{3}{2})^{1/2}\left[\int_{\phi_{mL}}^{\phi_L} d\phi\frac{1}{(\phi^3 - \phi_{mL}^3)^{1/2}} + \int_{\phi_{mL}}^{\phi_{L+1}} d\phi\frac{1}{(\phi^3 - \phi_{mL}^3)^{1/2}}\right], \tag{19}$$

where $d = |\xi_L^- - \xi_{L+1}^+|$ is the distance (corresponding to nc_0 in z space) between two neighboring intercalant layers.

Defining

$$f(x) = (\tfrac{3}{2})^{1/2}\int_x^1 dy\frac{1}{[y(1-y^3)]^{1/2}}, \tag{20}$$

we rewrite (18) and (19) as

$$(\phi_s)^{1/2}s = f(\phi_s/\phi_1), \tag{21}$$

$$f(\phi_{mL}/\phi_{L+1}) = (\phi_{mL})^{1/2}d - f(\phi_{mL}/\phi_L), \tag{22}$$

and (17) as

$$\phi_{mL+1} = \{\phi_{L+1}^3 - [(\tfrac{3}{2})^{1/2}p - (\phi_{L+1}^3 - \phi_{mL}^3)^{1/2}]^2\}^{1/3}. \tag{23}$$

Thus (21)–(23) are our iteration equations. We try a value of ϕ_s, and obtain ϕ_1 from (21), then use (23) and (22) repeatedly to find ϕ_{m1}, ϕ_2, ϕ_{m2}, ϕ_3, etc. The iteration of ϕ_{ml} (or ϕ_L) should tend gradually towards the bulk solution ϕ_{mb} (ϕ_b); otherwise the initial value ϕ_s should be adjusted until a proper ϕ_s is found. ϕ_{mb} and ϕ_b are determined by numerically solving the following two equations:

$$2[\tfrac{2}{3}(\phi_b^3 - \phi_{mb}^3)]^{1/2} = p, \tag{24}$$

$$d = 2(\tfrac{3}{2})^{1/2}\int_{\phi_{mb}}^{\phi_b} d\phi\frac{1}{(\phi^3 - \phi_{mb}^3)^{1/2}}. \tag{25}$$

Having found ϕ_s, we use the Runge-Kutta numerical method for solving the initial value problem for the differential equation (15) to find $\phi(\xi)$ in the surface region ($o \le \xi \le s$, or $0 \le z \le mc_0$), and hence the potential distribution $V(z)$ among the m surface graphite layers.

The above treatment can be easily extended to the case of acceptor GIC's. The form of $V(z)$ obtained is the same as for donors except for the sign.

Since we treat the intercalant layers as uniformly charged sheets, the model Hamiltonian (see below) does not reflect superlattice effects (due to the in-plane intercalate periodicity being different from that of the graphite). This simplification appears to be a reasonable one since Selloni and co-workers,[15] who carred out detailed pseudopotential calculations for the case of stage-1 LiC_6, found the superlattice effects on the STM corrugation amplitude to be very small. Note, however, that some very recent experiments carried out by Kelty and Lieber[14] in an argon atmosphere suggest that in some state-1 alkali-metal GIC's such superlattice effects may be observable.

B. Tight-binding H matrix

In our tight-binding model Hamiltonian of the graphite layers we follow Blinowski and co-workers[22] by including only the nearest-neighbor in-plane and interlayer hopping terms. All electronic hopping terms between host layers separated by a guest layer are ignored. For a single graphite layer, as there are two atoms per unit cell, the wave function with wave vector **k** is constructed using two tight-binding basis functions $u_{ik}(\mathbf{r})$ built of atomic $2p_z$ orbitals $\varphi_z(\mathbf{r})$. For a system of m graphite layers, the wave function Ψ_k is then a linear combination of $2m$ tight-binding basis functions[22]

$$u_{ik}(\mathbf{r}) = C\sum_{\mathbf{R},n}\exp[i\mathbf{k}\cdot(\mathbf{R}_n + \tau_i)]\varphi_z(\mathbf{r} - \mathbf{R}_n - \tau_i), \tag{26}$$

$$\Psi_k(\mathbf{r}) = \sum_i a_{ik}u_{ik}(\mathbf{r}) \quad (i = 1, 2, \ldots, 2m), \tag{27}$$

where C is the normalizing factor, **k** is the 2D wave vec-

tor, and $\mathbf{R}_n = n_1\mathbf{A}_1 + n_2\mathbf{A}_2$ is the 2D lattice vector formed from primitive translation vectors $\mathbf{A}_1$ and $\mathbf{A}_2$. τ_{2j-1} and τ_{2j} ($j=1,2,\ldots,m$) are the shortest vectors from the origin $\tau_1=0$ (see Fig. 2) to α- and β-type atoms,

respectively, in the jth graphite layer.

In the basis defined by Eq. (26) our approximate Hamiltonian for an $m=4$ surface domain is represented by the following matrix:

$$
\begin{vmatrix}
H_{11}\pm\Delta_1 & -\gamma_0 g(\mathbf{k}) & \gamma_1 & 0 & 0 & 0 & 0 & 0 \\
-\gamma_0 g^*(\mathbf{k}) & H_{11}\pm\Delta_1 & 0 & 0 & 0 & 0 & 0 & 0 \\
\gamma_1 & 0 & H_{11}\pm\Delta_2 & -\gamma_0 g^*(\mathbf{k}) & \gamma_1 & 0 & 0 & 0 \\
0 & 0 & -\gamma_0 g(\mathbf{k}) & H_{11}\pm\Delta_2 & 0 & 0 & 0 & 0 \\
0 & 0 & \gamma_1 & 0 & H_{11}\pm\Delta_3 & -\gamma_0 g(\mathbf{k}) & \gamma_1 & 0 \\
0 & 0 & 0 & 0 & -\gamma_0 g^*(\mathbf{k}) & H_{11}\pm\Delta_3 & 0 & 0 \\
0 & 0 & 0 & 0 & \gamma_1 & 0 & H_{11}\pm\Delta_4 & -\gamma_0 g^*(\mathbf{k}) \\
0 & 0 & 0 & 0 & 0 & 0 & -\gamma_0 g(\mathbf{k}) & H_{11}\pm\Delta_4
\end{vmatrix}, \qquad (28)
$$

where Δ_j represents the potential energy in graphite layer j, which is determined by averaging the self-consistent screened potential energy $eV(z)$ over the range of c_0 occupied by the jth layer, $g(\mathbf{k}) = \exp(i\mathbf{k}\cdot\tau_2) + \exp(i\mathbf{k}\cdot D_3\tau_2) + \exp(i\mathbf{k}\cdot D_3^{-1}\tau_2)$,[22] and D_3 is the operator of the $2\pi/3$ rotation about the c axis; γ_0 is the resonance integral[22] between the carbon $2p_z$ orbitals of nearest-neighbor α-β atoms within a graphite layer, while γ_1 is that between the orbitals of nearest-neighbor α-α atoms on adjacent graphite layers. We take $\gamma_0=2.51$ eV and $\gamma_1=0.377$ eV.[24] The "$+$" sign is for the case of acceptor guests and the "$-$" sign for the case of donor guests. All matrix elements between two carbon atoms separated more than the distance c_0 are neglected. Also, all matrix elements between graphite layers separated by a guest layer and between graphite and guest layers are neglected.

Shifting all energy levels by $H_{11}\pm\Delta_1$, we write the secular equation of the matrix (28) as

$$
\begin{vmatrix}
-E & -x & \gamma_1 & 0 & 0 & 0 & 0 & 0 \\
-x^* & -E & 0 & 0 & 0 & 0 & 0 & 0 \\
\gamma_1 & 0 & -(E\pm\delta_{12}) & -x^* & \gamma_1 & 0 & 0 & 0 \\
0 & 0 & -x & -(E\pm\delta_{12}) & 0 & 0 & 0 & 0 \\
0 & 0 & \gamma_1 & 0 & -(E\pm\delta_{13}) & -x & \gamma_1 & 0 \\
0 & 0 & 0 & 0 & -x^* & -(E\pm\delta_{13}) & 0 & 0 \\
0 & 0 & 0 & 0 & \gamma_1 & 0 & -(E\pm\delta_{14}) & -x^* \\
0 & 0 & 0 & 0 & 0 & 0 & -x & -(E\pm\delta_{14})
\end{vmatrix} = 0, \qquad (29)
$$

where $\delta_{1j}=\Delta_1-\Delta_j$ is the potential-energy difference between the first graphite layer and the jth layer, which is always a positive value, and x represents $\gamma_0 g(\mathbf{k})$.

For $m<4$ surface domains, the H matrices are simply the upper-left $2m\times 2m$ parts of the $m=4$ matrix.

Thus, in our model the presence of the intercalate is felt only through its influence on the site-diagonal Hamiltonian matrix elements δ_{1j} ($j=2,3,\ldots,m$) and on the total number of electrons present. The former are very sensitive to the charge-transfer value $2f/q$ and to m, and the latter is ultimately determined by the value $2f/q$.

Using as input the results of the self-consistent Thomas-Fermi calculation of $V(z)$ described in Sec. II A, we find the matrix elements of the tight-binding Hamiltonian of the m surface graphite layers. We then solve the secular equation (29), determine the energy bands and the Fermi level, and evaluate $\rho(\mathbf{r},E_F)$ using Herman-Skillman tight-binding carbon orbitals.[26]

IV. RESULTS

In Fig. 4 we show the calculated constant-current STM profiles for a typical acceptor GIC, stage-4 $SbCl_5$-graphite, with stoichiometry $SbCl_5 C_{14\times 4}$ and charge-transfer coefficient $f=0.31$ ($2f/q=0.31/7$).[27] $SbCl_5$-graphite is of particular interest because of the previous experimental observation of the surface domain structure in that system.[19] The results for a stage-4 alkali-metal donor GIC with stoichiometry $MC_{6\times 4}$ and $f=1$ ($2f/q=\frac{1}{3}$) are shown in Fig. 5. $MC_{6\times 4}$ is a donor GIC with a high areal density of transferred charge. Among alkali-metal GIC's only Li-graphite has equilibrium phases with a bulk stoichiometry of $MC_{6\times n}$ at ambient pressures, the other alkali metals being more dilute. However, guest concentrations as high as MC_6 in the first subsurface gallery have been reported for the other alkali metals.[20] While the results shown in Figs. 4 and 5 are for
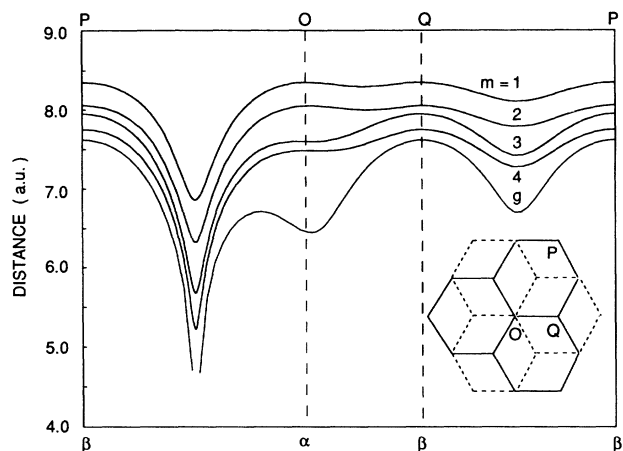
FIG. 4. Calculated constant-current STM profiles for stage-4 SbCl$_5$-graphite surfaces (curves 1–4 correspond to $m = 1$–4 graphite layers covering the top guest layer as in Fig. 1), and for a four-layer slab of pristine graphite (curve g). For curve g the Fermi energy was taken to be 0.0258 eV to reflect in a rough way the thermal broadening of the Fermi surface as discussed in Ref. 5. The scans shown are along *PO-OQ-QP* in the inset. Inset: Structure of the surface graphite layer (solid hexagons), and (for cases $m = 2$–4) of the first subsurface graphite layer (dashed hexagons). No corrections for finite instrumental resolution are included.

stage-4 compounds, the calculated profiles are very insensitive to the bulk stage, and reflect mainly the number of graphite layers covering the guest layer closest to the surface, and the in-plane density σ or the $2f/q$ of that guest layer. The physical origin of the insensitivity to the bulk stage is that the influence of the second guest layer from the surface is very weak because of the screening effects.[18] Thus the results presented are also representative of other bulk stages with similar in-plane densities.

In Figs. 4 and 5, the vertical axis represents the distance from the center of curvature of the tip to the plane containing the carbon nuclei in the surface graphite layer. The horizontal axis stands for the surface coordinate.
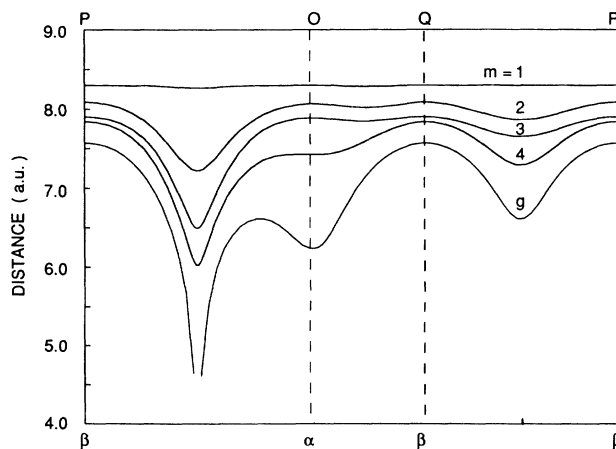

FIG. 5. Calculated constant-current STM profiles for stage-4 $MC_{6\times4}$ alkali-metal–graphite surfaces and for pristine graphite. Notation as in Fig. 4.

Curves 1–4 in each figure correspond to $m = 1$–4 graphite layers at the surface covering the top guest layer as in Fig. 1. Curve g, shown for comparison, is the result for a four-layer slab of pristine graphite. The scanning path across the surface is along the line *PO-OQ-QP* as defined in the inset of Fig. 4. The points labeled α and β on the horizontal axis mark the locations of the α and β atoms of the surface graphite layer. The five curves in each figure correspond to the same tunneling current. With increasing m, the charge density on the top surface layer decreases due to the screening, so that the tip has to be closer to the surface in order to deep the same tunneling current. Thus the curves shift to lower distance with increasing m in the figures.

A striking feature of the STM profiles shown in Figs. 4 and 5 is the marked reduction in the strength of the depression at the center of the carbon hexagon upon intercalation. This is due to the fact that the Fermi surface of the graphite is greatly expanded by the carriers transferred from the guest, so that the wave functions of the Fermi electrons no longer have an exact node at the hexagon center, as was anticipated by Tersoff.[5] The increase in the strength of the depression as the number of host layers m between the first guest layer and the surface increases can be understood qualitatively as an effect of the screening of the guest layer by the transferred charge: The further the surface graphite layer is from the guest layer, the less the free-carrier density at the surface and the more the STM image resembles that of pristine graphite. The depression in the profile is weaker for a given value of m in Fig. 5 than in Fig. 4 for two reasons: (a) there is a higher density of transferred charge in the former case, and (b) the linear combination coefficients $a_{i\mathbf{k}}$ which determine the form of the electron eigenfunctions $\Psi_\mathbf{k}$ are different for donor and acceptor guests in such a way that the corrugations are weaker for donors than for acceptors even when the $2f/q$ and the shape of the Fermi surface (but not the Fermi level) are the same.

The combination of these effects is so strong when there is only one graphite layer covering the alkali-metal guest (curve $m = 1$, Fig. 5) that the STM image is predicted to be nearly featureless on the atomic scale. Thus we are able to explain the quite remarkable absence of atomic scale features in the STM image of the BiCs-graphite reported recently by Gauthier *et al.*[11] if, as was noted by those authors, there is a high concentration of Cs in the first subsurface gallery of their samples due to segregation effects.[11]

The calculated corrugation amplitudes increase by about 20% if the average tip-to-surface separation is decreased by 2.5 a.u. (see Figs. 2 and 3 in Ref. 16), but the carbon-atom site asymmetry values do not show strong dependence on the tip separation.

The behavior of the asymmetry between the α and β carbon-atom sites is very interesting. There is no hint of any asymmetry for $m = 1$ or 2 in Fig. 4 or for $m = 1$, 2, or 3 in Fig. 5. This is a surprise since bilayers and trilayers of *AB*-stacked pristine graphite display a strong asymmetry. Recently Tománek and Louie[8] have pointed out that in stage-1 alkali-metal GIC's which have *A A* stacking there should be no carbon-atom asymmetry since the

asymmetry is linked to AB stacking. Here we predict that the asymmetry should be absent for small numbers of graphite layers covering the first guest layer, *even for AB stacking*. One can think of this very roughly as follows. The coupling between adjacent graphite layers is the reason why the carbon-atom site asymmetry (CSA) in the STM image of pristine graphite is linked to AB stacking. The coupling is stronger at α sites than β sites since the distance between the nearest-neighbor α-α sites on adjacent layers is the shortest one. Therefore, on the top surface layer the electrons on the α atoms have the larger probability of being attracted downward due to the coupling with the layer underneath, so that the β atoms are more visible in the STM image. When we intercalate some guests, say, acceptors, the charge-transfer effect will cause carbon atoms to lose electrons. The electrons on the β atoms are somewhat less tightly bound to their sites and thus have the greater probability of being taken up by the intercalate. If the charge transfer is strong enough, it is possible to greatly reduce the difference between α and β sites in the STM image. This is a *very* rough and intuitive explanation; a more detailed explanation of the absence of CSA based on the properties of the system wave functions, the energy band structure, and the Fermi surface will be given below.

The asymmetry appears *abruptly* at $m = 3$ in Fig. 4 and at $m = 4$ in Fig. 5, but is weaker than in pristine graphite. This is quite different from the behavior of the corrugation hole at the center of the carbon hexagon which never disappears totally and grows *smoothly* with increasing m. We find that the finite asymmetry appears *discontinuously* with decreasing charge transfer at fixed $m > 1$, when the highest electron (deepest hole) surface subband is emptied of electrons.

In Fig. 6(a) we show the calculated carbon-atom site asymmetry versus $2f/q$ for $m = 2$ surface domains. The CSA value is the height difference between α and β sites in the STM image. Curves D and A represent donor and acceptor guest GIC's, respectively, with the same constant tunneling current. In the figure, there is a point at which the CSA switches on from zero to a finite value. The corresponding $2f/q$ is about 0.034 which varies very slightly (by $\leq 5\%$) with the bulk stage. As the STM probes the local electron density of states at the Fermi level, the discontinuity should be linked with the energy band structure and the Fermi level of the system. Figures 7(a) and 7(b) show the energy bands of pristine graphite bilayers and the $m = 2$ surface domain of a donor GIC at the onset of the CSA with $\theta = 0$, respectively. Notice that the Fermi level coincides with the bottom of the highest electron surface subband in Fig. 7(b). Consider the situation at $\kappa = 0$, the corner of hexagonal 2D Brillouin zone [see Fig. 2(c)]. There $g(\mathbf{k}) = 0$, and the $m = 2$ secular equations are

$$-a_1 E + a_3 \gamma_1 = 0 ,$$

$$-a_2 E = 0 ,$$

$$-a_1 \gamma_1 - a_1 (E - \delta_{12}) = 0 ,$$

$$-a_4 (E - \delta_{12}) = 0 .$$

(30)

For pristine graphite bilayers, $\delta_{12} = 0$, and $E_F = 0$ as shown in Fig. 7(a). Then from (30) we find $a_1 = a_3 = 0$, but a_2 and a_4 are not equal to zero. From Fig. 2(b) it is clear that this means that the Fermi electron wave function vanishes on the α sites. The tunneling current is therefore contributed only by β-type atoms, implying a strong CSA. By contrast, for a donor GIC at the CSA
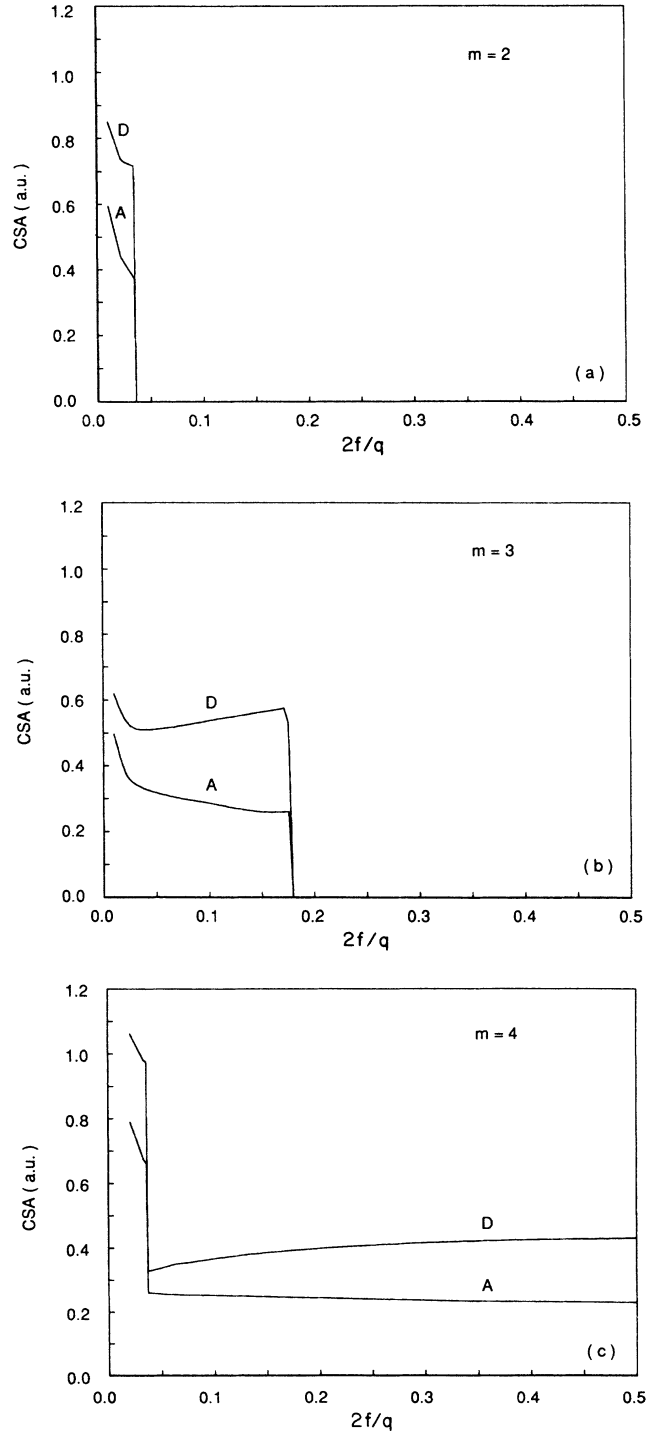

FIG. 6. The calculated curves of carbon-atom site asymmetry vs $2f/q$ for (a) $m = 2$, (b) $m = 3$, and (c) $m = 4$. A denotes acceptor, D denotes donor.

onset, the E_F just approaches the bottom of the highest electron surface subband E_{C1}. Since in this case $E_F > \delta_{12}$, it follows from (30) that for states at the bottom of this subband $a_2 = a_4 = 0$, but a_1 and a_3 are not equal to zero. This means that the subband E_{C1} strongly favors the α sites. Since the lower conduction surface subband E_{C2} also has many states at the Fermi level, and this subband strongly favors β sites, by adding these two parts we get the tunneling current contributed not only by β-type but also by α-type atoms, implying a greatly reduced CSA. The higher conduction surface subband is parabolic at its extremum, which implies that (in two dimensions) it has a nearly constant density of states. Thus its contribution to the tunneling current (which strongly favors the α site)

switches off discontinuously as it empties, which explains how it is possible for the asymmetry to be a discontinuous function of the Fermi level, or of the $2f/q$. The calculated results show that there is no CSA when $E_F \geq E_{C1}$ ($\kappa = 0$).

We find that the energy bands of an acceptor GIC are simply the mirror image of those of the donor GIC with the same $2f/q$ and the Fermi level is the same in magnitude and differs only in its negative sign. That is why both kinds of GIC's have the common CSA onset.

From (30) we can obtain analytically the condition for the absence of CSA for donor GIC's in the case of $m = 2$: $E_F \geq [\delta_{12} + (\delta_{12}^2 + 4\gamma_1^2)^{1/2}]/2$. Similarly, for acceptor GIC's the condition is $E_F \leq -[\delta_{12} + (\delta_{12}^2 + 4\gamma_1^2)^{1/2}]/2$.
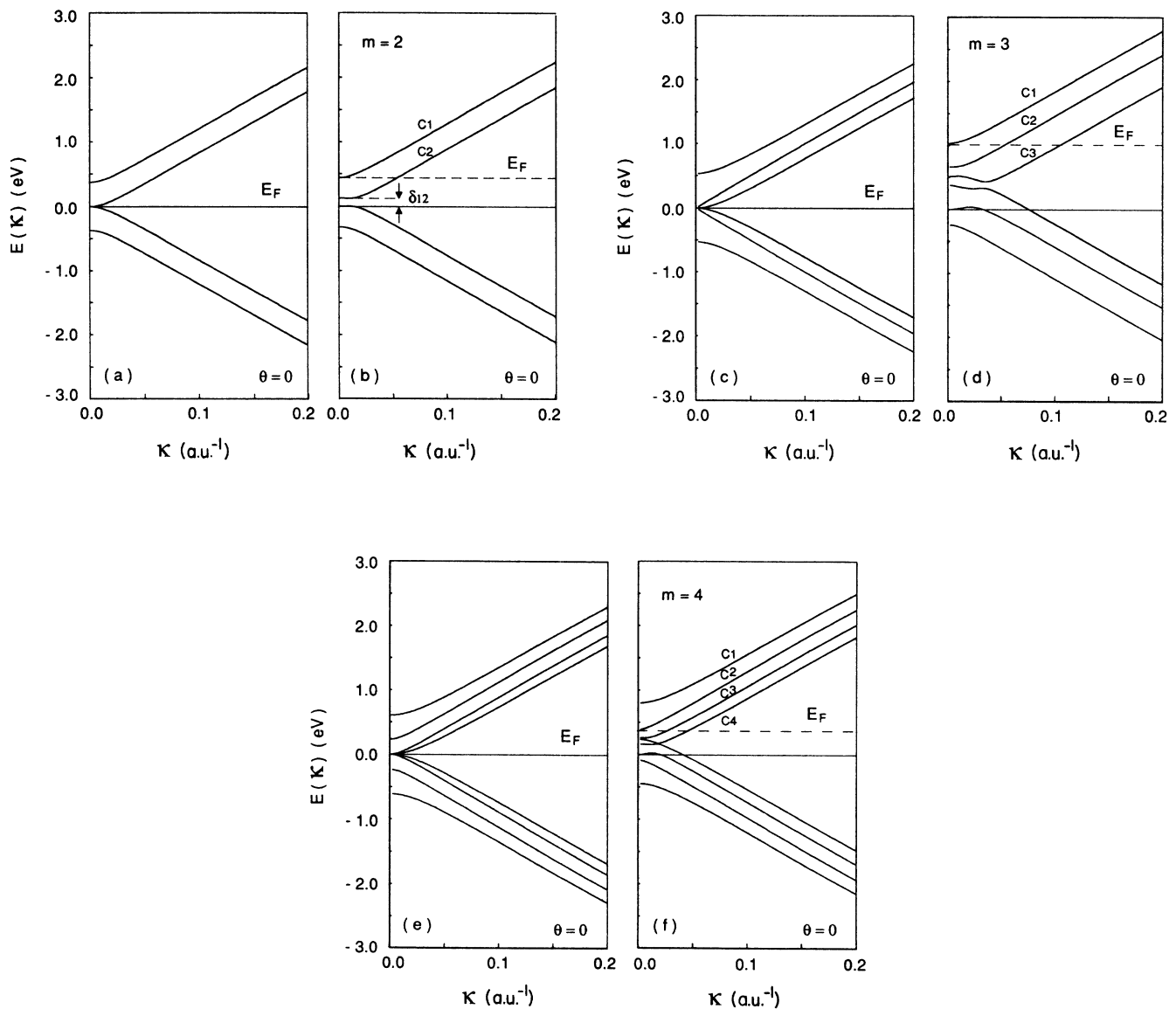

FIG. 7. The energy band structure of m graphite layers with $\theta = 0$ (the band structure will change somewhat with θ, but the relative locations of subbands are always close to that shown). Pristine graphite bilayers, trilayers, and four-layers in (a), (c), and (e), respectively. $m = 2$–4 surface domains of donor GIC's at the CSA onsets in (b) and (d), and discontinuity in (f), respectively. $2f/q$ values are 0.034, 0.175, and 0.037 in (b), (d), and (f), respectively.
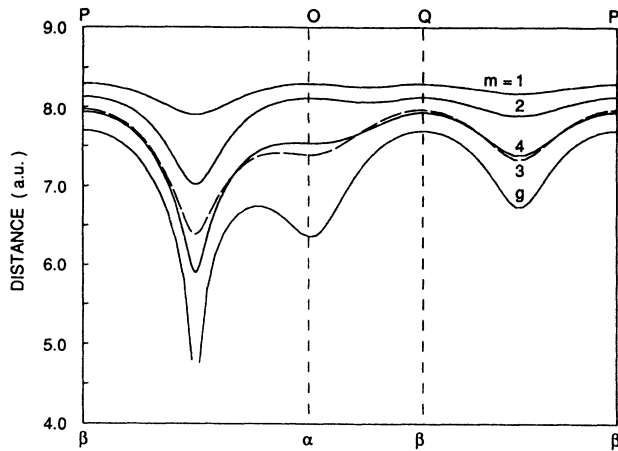
FIG. 8. Calculated constant-current STM profiles for stage-4 $MC_{12\times4}$ alkali-metal–graphite surfaces and for pristine graphite. Notation as in Fig. 4.

The CSA versus $2f/q$ is plotted for $m=3$ and 4 cases in Figs. 6(b) and 6(c), and the respective energy bands in Figs. 7(c) and 7(d), and 7(e) and 7(f). In Fig. 6(b), the onset for $m=3$ is at about 0.175, which is much larger than the value for $m=2$. This is reasonable since the screening of the first guest layer increases with m, and the larger m is the less the charge transfer affects the top surface. In Fig. 6(c) the screening for $m=4$ is so strong that there is some CSA even when $2f/q$ reaches 0.5. But notice that the CSA jumps from a lower to a higher value when the second conduction subband empties as shown in Fig. 7(f). This occurs at a $2f/q$ of about 0.037, and the conditions of a lower value of the CSA are that $E_F \geq E_{c2}$ ($\kappa=0$) for donors and $E_F \leq -E_{c2}$ ($\kappa=0$) for acceptors.

In general, the $2f/q$ at the CSA onset increases with m because of the effects of screening. The overall trend is for the CSA to increase with decreasing $2f/q$, but some deviations from this do occur. The difference between donor and acceptor asymmetry values tends to decrease with $2f/q$. It is zero for $2f/q=0$, i.e., for pristine graphite. For a fixed $2f/q$ the donor CSA is always larger than the acceptor CSA; this is because the form of Ψ_k is different for donor and acceptor GIC's even though their Fermi surfaces are the same.

It is interesting to see from Fig. 6 that for some GIC's the CSA may be *larger* for smaller m. Figure 8 shows the STM images of $m=1-4$ domains for stage-4 $MC_{12\times4}$ with $2f/q=\frac{1}{6}$. The asymmetry *decreases* significantly from $m=3$ (dashed line) to $m=4$. The reason is that the different surface subbands contribute differently to the asymmetry strength, so that their number and character and the location of the Fermi level *relative to them* are all important *and change with m*. It is clear that careful asymmetry measurements would be very interesting.

An excellent way to test our predictions experimentally would be to map out the surface domain structure of a freshly cleaved stage GIC, since different domains with different m values should have differing corrugation strengths and carbon-atom site asymmetries, as well as having their surfaces offset vertically from each other[17] because of the bends in the graphite layers at the domain walls.

V. CONCLUSIONS

We have developed a theory of the STM images of the surfaces of staged graphite intercalation compounds. The number m of graphite layers covering the first guest layer and the charge-transfer value are the important parameters entering our theory. We determine the transferred charge distribution along the c-axis, the surface energy bands, and the Fermi level by using the Thomas-Fermi equations of Safran and Hamann and a modification of the tight-binding model of Blinowksi and co-workers, and calculate the constant-current-mode STM image using the Tersoff and Hamann theory. We find that the corrugation amplitude and carbon-atom site asymmetry are very sensitive to the m and the charge transfer, but insensitive to the bulk stage due to the screening of intercalant layers. The corrugation amplitude increases with increasing m, with decreasing charge transfer, and also with decreasing tip-to-surface separation. The asymmetry does not strongly depend on the tip-to-surface separation, but has a surprising dependence on the charge transfer and m, switching on discontinuously with decreasing charge transfer. We predict that in many cases there should be no carbon-atom site asymmetry in the STM image even when the usual AB stacking of the graphite layers occurs at the GIC surface.[28] For a given charge transfer, the corrugation amplitude is larger for acceptor GIC's and the asymmetry is larger for donor GIC's. Our calculations explain the unusual absence of atomic-scale features in the STM images of BiCs-graphite recently reported by Gauthier and co-workers,[11] and the results for pristine graphite are in good agreement with those obtained using different theoretical methods. Our results for GIC's can be used to map the stage domains across a freshly cleaved surface and our predictions should stimulate further experimental and theoretical work in this interesting new area of surface science. Such studies will also help to clarify some currently controversial issues about the bulk properties of intercalation compounds.

ACKNOWLEDGMENTS

[1]G. Binnig and H. Rohrer, IBM J. Res. Dev. **30**, 355 (1986).

[2]P. K. Hansma and J. Tersoff, J. Appl. Phys. **61**, R1 (1987).

[3]A. Selloni, P. Carnevali, E. Tosatti, and C. D. Chen, Phys. Rev. B **31**, 2602 (1985).

[4]G. Binnig, H. Fuchs, Ch. Gerber, H. Rohrer, E. Stoll, and E. Tosatti, Europhys. Lett. **1**, 31 (1986).

[5]J. Tersoff, Phys. Rev. Lett. **57**, 440 (1986).

[6]I. P. Batra, N. Garcia, H. Rohrer, H. Salemink, E. Stoll, and S.

Ciraci, Surf. Sci. **181**, 126 (1987).

[7]D. Tomanek, S. G. Louie, H. J. Mamin, D. W. Abraham, R. E. Thomson, E. Ganz, and J. Clarke, Phys. Rev. B **35**, 7790 (1987).

[8]D. Tomanek and S. G. Louie, Phys. Rev. B **37**, 8327 (1988).

[9]See *Graphite Intercalation Compounds, Springer Topics in Current Physics,* edited by H. Zabel and S. A. Solin (Springer, New York, in press).

[10]M. S. Dresselhaus and G. Dresselhaus, Adv. Phys. **30**, 139 (1981).

[11]S. Gauthier, S. Rousset, J. Klein, W. Sacks, and M. Belin, J. Vac. Sci. Technol. A **6**, 360 (1988).

[12]M. Tanaka, W. Mizutani, T. Nakashizu, N. Morita, S. Yamazaki, H. Bando, M. Ono, and K. Kajimura, J. Microsc. **152**, 183 (1988).

[13]D. Anselmetti, R. Wisendanger, V. Geiser, H. R. Hidber, and H. J. Güntherodt, J. Microsc. **152**, 509 (1988); D. Anselmitti, R. Weisendanger, and H. J. Güntherodt, Phys. Rev. B **39**, 11 135 (1989).

[14]S. P. Kelty and C. M. Lieber, Phys. Rev. B **40**, 5856 (1989).

[15]A. Selloni, C. D. Chen, and E. Tosatti, Phys. Scr. **38**, 297 (1988).

[16]A preliminary account of some of our results has already been published; see X. Qin and G. Kirczenow, Phys. Rev. B **39**, 6245 (1989).

[17]See S. E. Ulloa and G. Kirczenow, Comments Condensed Matter Phys. **12**, 181 (1986).

[18]S. A. Safran and D. R. Hamann, Phys. Rev. B **22**, 606 (1980).

[19]R. Levi-Setti, G. Crow, Y. L. Wang, N. W. Parker, R. Mittle-man, and D. M. Hwang, Phys. Rev. Lett. **54**, 2615 (1985).

[20]M. Laguës, D. Marchand, and C. Frétigny, Solid State Commun. **59**, 583 (1986).

[21]J. Tersoff and D. R. Hamann, Phys. Rev. B **31**, 805 (1985).

[22]J. Blinowski and C. Rigaux, Synth. Met. **2**, 297 (1980); J. Blinowski, N. H. Hau, G. Rigaux, J. P. Vieren, R. L. Toullec, G. Furdin, A. Hérold, and J. Melin, J. Phys. (Paris) **41**, 47 (1980).

[23]R. Nishitani, Y. Uno, and H. Suematsu, Phys. Rev. B **27**, 6572 (1983); Y. Yosida, K. Sato, K. Suda, and H. Suematsu, J. Phys. Soc. Jpn. **55**, 561 (1986).

[24]Y. Yosida and S. Tanuma, Synth. Met. **23**, 199 (1988).

[25]The numerical results presented in this paper are for a model in which the intercalate layers are represented by charged sheets of infinitesimal thickness so that electrostatic boundary conditions at the graphite-intercalate interfaces take a simple form [Eqs. (12) and (13)]. We have also carried out more detailed calculations in which finite intercalate thicknesses typical of various GIC's are assumed and have found the effect on the calculated STM images to be very small (<0.01 a.u.), justifying the above idealization.

[26]F. Herman and S. Skillman, *Atomic Structure Calculations* (Prentice-Hall, Englewood Cliffs, NJ, 1963).

[27]D. M. Hwang, X. W. Qian, and S. A. Solin, Phys. Rev. Lett. **53**, 1473 (1984).

[28]The only published experimental study to date (Ref. 14) which has attempted to address the question of carbon-atom site asymmetry for stages higher than 1 did not observe this predicted anomalous behavior; further experimental work on this problem, preferably in vacuum, would be of interest.
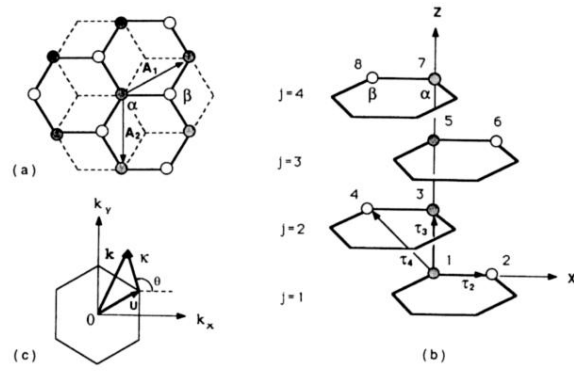
FIG. 2. Graphite AB stacking structure with α- and β-type carbon-atom sites in (a) 2D and (b) 3D perspectives, and (c) the hexagonal 2D Brillouin zone, where wave vector $\mathbf{k} = \mathbf{u} + \boldsymbol{\kappa}$ and $\mathbf{u} = (2\pi/3b, 2\pi/3^{3/2}b)$.
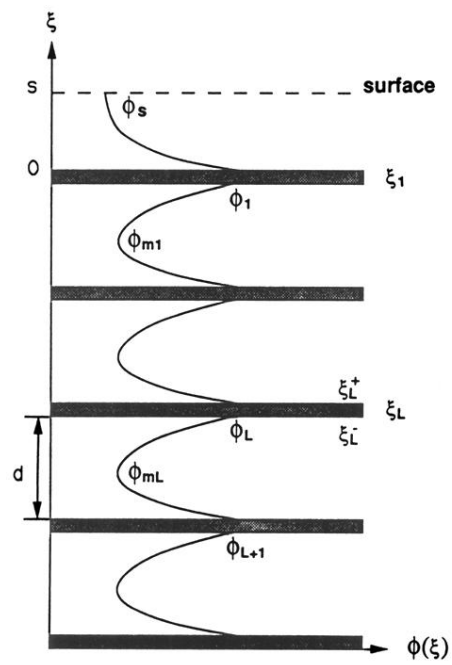
FIG. 3. Schematic representation of the charge-transfer-associated potential-energy distribution between intercalant layers and between the surface and the first subsurface intercalant layer.